CURE INDUCED MULTI-AXIAL STRAIN DEVELOPMENT IN CURVD COMPOSITE COMPONENTS: FIBER-OPTIC-BASED MONITORING AND NUMERICAL ANALYSIS

Kazunori Takagaki[1], Shu Minakuchi[2] and Nobuo Takeda[3]

[1-3]Department of Advanced Energy, Graduate School of Frontier Sciences, The University of Tokyo,
5-1-5, Kashiwanoha, Kashiwa, Chiba 277-8561, Japan,
Web Page: http://www.smart.k.u-tokyo.ac.jp
E-mail: [1]takagaki@smart.k.u-tokyo.ac.jp, [2]minakuchi@smart.k.u-tokyo.ac.jp,
[3]takeda@smart.k.u-tokyo.ac.jp,

Keywords: Curved Composites, Cure Induced Strain/Distortion, Optical Fiber Sensors, In-Situ Monitoring, Finite Element Analysis

Abstract
Curved composite parts have been widely used for a variety of industries. However, cure induced residual deformation (i.e., spring-in) occurs in such components. Though lots of works have investigated the deformation, fundamental mechanisms are still unclear because internal state measurement methods have not been developed. Thus, the current research aims to establish an in-situ strain measurement technique especially for the out-of-plane normal and shear strains. Two L-shaped specimens with different thickness were fabricated and optical fiber sensors were diagonally embedded into the specimens to monitor strains during cure. The normal and shear strains and shear/normal strain ratio were calculated from the sensor responses, indicating larger shear strain in the thick specimen. 3D scanning showed smaller spring-in in the thick specimen. In addition, numerical analysis confirmed the validity of the measurements. This research experimentally and numerically revealed that larger shear strain is generated in thicker specimens, suppressing the residual deformation. The proposed technique will be utilized to explore other effect like cure conditions.

1. Introduction

Carbon fiber reinforced plastic (CFRP) is an attractive alternative to the conventional metal material due to its advantages: high specific strength/stiffness and low density. As CFRP has been used for a variety of industries including aerospace, cars and sport infrastructures, more complex shaped CFRP has been required. Among them, L-shaped composites are one of the most fundamental components. However, cure induced deformation (i.e., spring-in) occurs in L-shaped composites due to its anisotropic nature, leading to strength reduction after assembly or troublesome shimming (Figure 1).

A lot of works have investigated spring-in deformation by experimental and analytical methods. Numerous experiments were carried out by Albert and Fernlund [1] and Kappel [2]. These researches found that larger spring-in is induced with thinner parts. Meanwhile, a simple theoretical model for spring-in prediction was proposed based on material anisotropy [3]:

$$\Delta\theta = \theta\left(\frac{(\alpha_l - \alpha_t)\cdot\Delta T}{1+\alpha_t\cdot\Delta T}\right) + \theta\left(\frac{\phi_l - \phi_t}{1+\phi_t}\right), \quad (1)$$

where θ is the part angle, α is the coefficient of thermal expansion, T is the temperature, ϕ is the chemical cure shrinkage, and subscripts l and t represent the longitudinal and transverse directions. This equation, however, does not include the effect of part thickness as indicated in the experiments

Excerpt from ISBN 978-3-00-053387-7

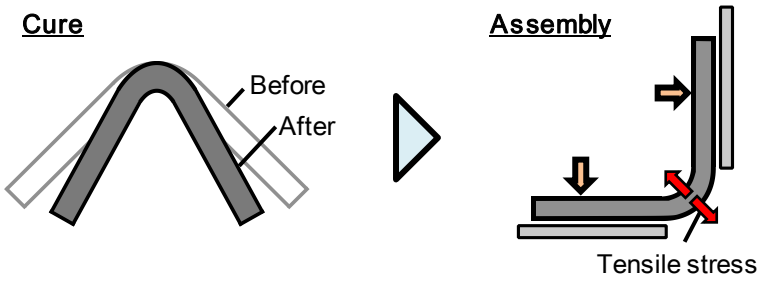

Figure 1. Schematic of spring-in induced during cure process, and accompanying through-thickness tensile stress generated during assembly.

[1,2]. Wisnom et al. [4] developed an analytical model based on the shear-lag analysis. The model showed that shear deformation occurs in a C-shaped composite when the part is in the rubbery state and the shear stiffness is low, resulting in smaller spring-in than predicted by Eq. 1. The analysis successfully predicted the effect of thickness that was observed in experiments. Detailed finite element simulations have been conducted to investigate several effects like resin states (i.e., viscous, rubbery and glassy) [5,6] and fiber wrinkle [7]. Despite these considerable researches over the past decades, the experiments contain several inconsistencies and fundamental mechanisms for spring-in are still unclear. For example, the effects of the part thickness and cure condition on the residual deformation are uncertain. It is partially because the previous researches mainly addressed the final cured shapes and internal state development during cure has not been measured.

This research aims to propose an in-situ multi-axial strain measurement technique and to investigate the effect of part thickness on the internal state and residual deformation. Optical fiber sensors are embedded into the ±45º diagonal directions to evaluate the normal and shear strains. In addition, numerical analysis is conducted to assess the validity of the experiment. The effect of the tool-part interaction was minimized by several techniques to focus on the effect of the cure induced chemical and thermal shrinkages.

2. Materials and Methods

2.1. Experiment

2.1.1. Optical Fiber Sensors

Optical fiber sensors are widely utilized for strain and temperature monitoring of composite materials due to their significant advantages: small diameter (less than 150 μm), light weight, corrosion resistance, immunity to electromagnetic interference and no need for electricity at sensing points [8]. Fiber Bragg grating (FBG) sensor is one of the optical fiber sensors and was chosen as the strain monitoring device in this research. An FBG sensor has local modulation in the refractive index along the length of an optical fiber. Figure 2 shows a schematic and principle of an FBG sensor. When broadband light is launched into the FBG sensor, a narrow spectrum is reflected back (Figure 2, Right). The center wavelength of the reflection spectrum is called Bragg wavelength, λ_b, and changes proportionally to axial strain and temperature at the grating area:

$$\Delta\lambda_0 = C_\varepsilon \Delta\varepsilon + C_T \Delta T, \quad (2)$$

where ε is the axial strain, T is the temperature, and C_ε and C_T are the coefficients. Strain change can be calculated from the wavelength change by compensating the temperature effect.
FBG sensors were embedded in the ±45º diagonal directions to monitor the out-of-plane normal and shear strain developments during cure process of L-shaped CFRPs. The FBGs were cut near the

Excerpt from ISBN 978-3-00-053387-7

grating area to be embedded in the diagonal directions. The distance between the grating area and the end of the optical fiber is called tail length [9]. It should be noted that the strain measured by the diagonal sensors with short tail length would be smaller than the strain induced in the CFRP parts due to the shear-lag effect near the end of the optical fiber especially when the resin has low stiffness [10]. The measured strain increment can be written as:

$$\Delta\varepsilon^{s} = \alpha(\mathbf{C}(t), l) \cdot \Delta\varepsilon^{c}, \tag{3}$$

where $\Delta\varepsilon^{s}$ are the strain increment measured in an FBG sensor, $\Delta\varepsilon^{c}$ is the strain increment induced in a composite part in the sensor direction, t is the time, and α is the shear-lag coefficient which depends on the stiffness of the composite $\mathbf{C}$ and the sensor tail length l. The shear-lag coefficient, α, increases from 0 to 1 with increasing stiffness $\mathbf{C}$ during cure. Meanwhile, the composite strains induced in the ±45° diagonal directions, ε^{c}_{+45} and ε^{c}_{-45}, is calculated by the in-plane strain, ε^{c}_{1}, the out-of-plane normal strain, ε^{c}_{2}, and the out-of-plane shear strain, ε^{c}_{12}, as:

$$\begin{aligned}\varepsilon^{c}_{+45} &= (\varepsilon^{c}_{1} + \varepsilon^{c}_{12} + \varepsilon^{c}_{2})/2 \cong (\varepsilon^{c}_{12} + \varepsilon^{c}_{2})/2 \\ \varepsilon^{c}_{-45} &= (\varepsilon^{c}_{1} - \varepsilon^{c}_{12} + \varepsilon^{c}_{2})/2 \cong (-\varepsilon^{c}_{12} + \varepsilon^{c}_{2})/2.\end{aligned} \tag{4}$$

The in-plane strain is assumed to be negligible since a cross-ply layup was used in this research. Eqs. 3 and 4 lead to strain increments measured in the ±45° diagonal sensors $\Delta\varepsilon^{c}_{+45}$ and $\Delta\varepsilon^{c}_{-45}$:

$$\begin{aligned}\Delta\varepsilon^{s}_{+45} &\cong \alpha(\mathbf{C}(t), l) \cdot (\Delta\varepsilon^{c}_{12} + \Delta\varepsilon^{c}_{2})/2 \\ \Delta\varepsilon^{s}_{-45} &\cong \alpha(\mathbf{C}(t), l) \cdot (-\Delta\varepsilon^{c}_{12} + \Delta\varepsilon^{c}_{2})/2.\end{aligned} \tag{5}$$

Summing the addition and subtraction of the measured strains (Eq. 5) gives values as:

$$\begin{aligned}\sum_{\tau}[\Delta\varepsilon^{s}_{+45}(\tau) + \Delta\varepsilon^{s}_{-45}(\tau)] &\cong \sum_{\tau}[\alpha(\tau) \cdot \Delta\varepsilon^{c}_{2}(\tau)] \stackrel{\text{def}}{=} \bar{\varepsilon}_{2}(t) \\ \sum_{\tau}[\Delta\varepsilon^{s}_{+45}(\tau) - \Delta\varepsilon^{s}_{-45}(\tau)] &= \sum_{\tau}[\alpha(\tau) \cdot \Delta\varepsilon^{c}_{12}(\tau)] \stackrel{\text{def}}{=} \bar{\varepsilon}_{12}(t),\end{aligned} \tag{6}$$

where τ is the dummy variable, t is the time and the tail length l is assumed to be the same for both the ±45° sensors. These values are defied as $\bar{\varepsilon}_{2}$ and $\bar{\varepsilon}_{12}$ as shown in Eq. 6, and they show the out-of-plane normal and shear strains reduced by the shear-lag coefficient of α. Though the reduced strains, $\bar{\varepsilon}_{2}$ and $\bar{\varepsilon}_{12}$, are not identical to the composite strains due to the shear-lag coefficient, they indicate qualitative trend for the composite strains. Moreover, Eq. 5 leads to the shear/normal composite strain ratio as:

$$\frac{\Delta\varepsilon^{c}_{12}(t)}{\Delta\varepsilon^{c}_{2}(t)} \cong \frac{\Delta\varepsilon^{s}_{+45}(t) - \Delta\varepsilon^{s}_{-45}(t)}{\Delta\varepsilon^{s}_{-45}(t) + \Delta\varepsilon^{s}_{-45}(t)}. \tag{7}$$

Note that this ratio is not affected by the shear-lag coefficient α, indicating that the composite internal state can be directly captured by the sensor responses. Furthermore, this ratio is a good indicator for the residual deformation because shear strain development would result in suppression of spring-in [4]. In the following experiment, the reduced out-of-plane normal and shear strains and the shear/normal strain ratio are calculated from the strains measured by diagonally embedded optical fibers.

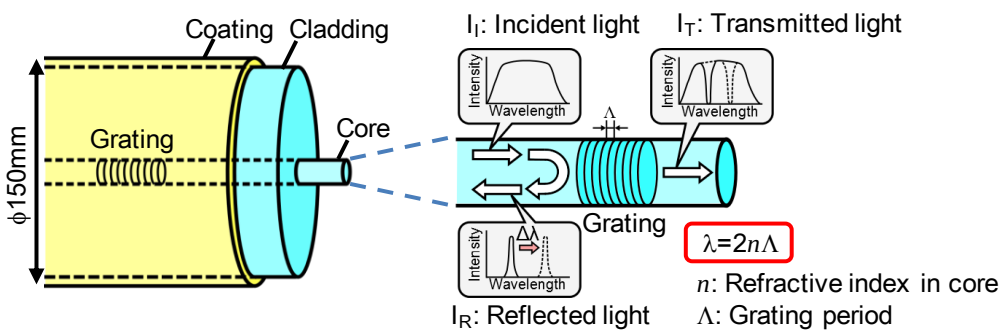

Figure 2. Structure and measurement principle of fiber Bragg grating (FBG) sensor.

Excerpt from ISBN 978-3-00-053387-7

2.1.2. Test Setup

Two L-shaped CFRP specimens were fabricated to investigate the effect of thickness on the internal strain induced during cure process. The stacking sequences of the specimens were $[0_2/90_4/0_4]_S$ (20-ply, thin; thickness: 2.5 mm) and $[90_4/0_4]_{4S}$ (64-ply, thick; thickness: 9 mm). The specimens had flange length of 45 mm and width of 70 mm. The material used was a CFRP prepreg: T700SC/2592 (Toray Industries, Inc.). Prepreg sheets were laid up onto an aluminum tool with corner radius of 6.4 mm. Two PTFE release films were placed between the tool and prepregs to minimize the tool-part interaction. After laying all the plies, holes were made in the ±45º directions using a needle with diameter of 1mm to embed FBG sensors. The hole depths were determined so that grating areas of FBG sensors were placed at the through-thickness center of the specimens. The holes were made at 25 mm from the corner and 30 mm from one another. Figure 3 shows a photograph and schematic of sensor embedment. The whole specimens were covered with glass fabric and bagging films and holes were made on the films as in the specimens. Two types of FBG sensors were used: one for the thin specimen had the tail length of 1.5 mm and grating length of 0.4 mm, and the other for the thick specimen had the tail length of 3 mm and grating length of 1 mm. These sensors were utilized to calculate the reduced strains and shear/normal strain ratio as shown in Eqs. 6 and 7. Though the difference in the tail length would affect the reduced strains given in Eq. 6, the shear/normal strain ratio in Eq. 7 is immune to the difference. The sensors were embedded into the specimens through the holes made on the bagging films. K-type thermocouples were embedded at the through-thickness center to measure temperature. The specimen was vacuumed and cured in an autoclave under a gage pressure of 0.3 MPa. The cure cycle includes 2 ºC/min heating, 90 ºC holding for 7 hours and 2 ºC /min cooling. During heating only 0.01 MPa vacuum and no autoclave pressures were applied to suppress the tool-part interaction. After reaching the curing temperature, full vacuum and autoclave pressures were applied. Moreover, both vacuum and autoclave pressures were released and re-applied immediately before the cooling phase. The FBG response and temperature were recorded at 2 min intervals throughout curing. After removing from the tool, 3D scanning using an instrument (ATOS; GOM mbH, Germany) was also carried out to measure the cured shape of the laminates.

2.2. Numerical Analysis

Finite element analysis (FEA) was conducted to further examine the process monitoring results using FEA software Abaqus 6.14. 1/4 thin (20-ply; thickness: 2.5 mm) and thick (64-ply; thickness: 9 mm) models were developed due to the symmetry of the L-shaped specimens and boundary conditions were applied to represent the whole L-shaped components (Figure 4 (a)). The stacking sequences were

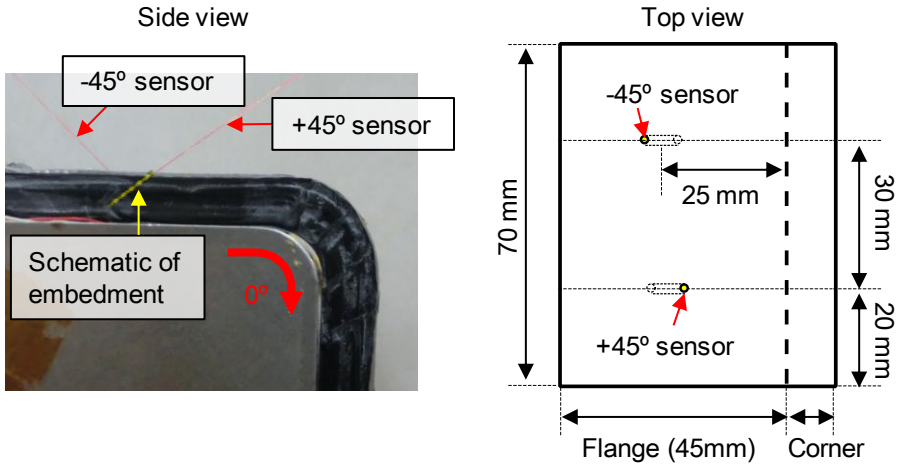

Figure 3. photograph (side view) and schematic (top view) of FBG sensor embedment.

Excerpt from ISBN 978-3-00-053387-7

the same as the experiment. The tool was modeled as a rigid shell and physical contact without friction was introduced between the tool and part because two PTFE films were used and quite low pressure was applied during heating in the experiment to minimize the tool-part interaction. Two step analysis was carried out assuming that material properties change from the rubbery to glassy state as a step transition [5]. In the first step, the resin was in the rubbery state and the composite properties were calculated using the self-consistent field model as a function of the Young's modulus of the resin, E_m [10]. The autoclave pressure was applied and shrinkage of 1000 με took place in the transverse directions. The stress/strain conditions induced in this step were frozen in using a user subroutine UMAT. In the second step, the resin vitrified and the properties of the glass state were used. The autoclave pressure was released and the part was allowed to deform freely. Additional shrinkage was not applied in this step. Five values of Young's modulus E_m were chosen for the first step: 5, 25, 50, 100, 3000 MPa. The last one was the same value as the fully cured one (glassy state), simulating cooling process. The effect of the Young's modulus on strains and cure induced deformation was evaluated (Figure 4 (b)).

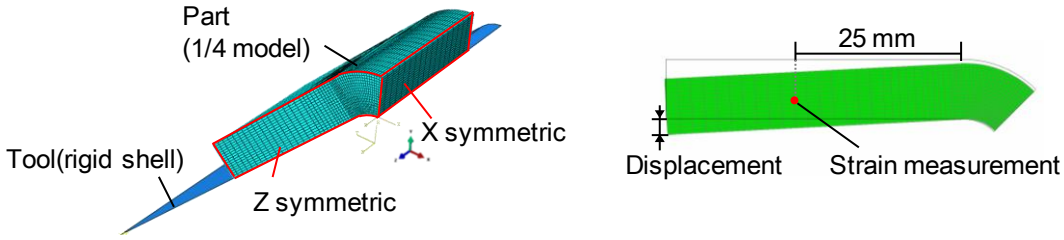

Figure 4. Finite element model: (a) Schematic of model and boundary conditions, (b) Strain measurement position and definition of displacement at edge.

3. Results and Discussion

Figure 5 (a) shows strain development in the thin specimen during the cure process. The strain at the gel point (200 min) was set to zero. Before gelation, strain changes due to resin movement and has insignificant effect on residual stress and deformation since the resin was in the liquid state with low stiffness. After gelation, compressive strain increased in both ±45º directions due to the chemical cure shrinkage. Although the two sensor responses changed differently in the beginning, similar trend was captured from the middle. Slight increase was observed in the +45º sensor upon the vacuum release before cooling. During cooling, compressive strains similarly increased in both of the directions due to the thermal shrinkage. Figure 6 gives the reduced out-of-plane normal and shear strains calculated from the ±45º sensor responses (Figure 5 (a)) using Eq. 6. Shear strain decreasing the +45º sensor strain was defined as negative value. Both the normal and shear strains significantly decreased from gelation to about 300 min. After 300 min, however, shear strain did not change though the normal strain continued to decrease gradually. As shear deformation is suppressed during curing, bending stress increases, resulting in larger spring-in deformation after demolding [4]. Therefore, this measurement result implies that the chemical cure shrinkage after 300 min caused significant residual deformation. During cooling, the compressive normal strain considerably increased compared with the shear strain. The measured spring-in angle was 0.51º for the thin specimen.

The monitored strain in thick specimen is shown in Figure 6 (a). Similarly to the thin specimen, the compressive strain increased after gelation. However, the difference between the two sensors during the 90 ºC dwell was larger than in the thin specimen. The compressive strain increased almost identically during cooling. Figure 6 (b) shows the reduced out-of-plane normal and shear strains in the thick specimen. Both the normal and shear strains considerably increased just after gelation and continued to change gradually until the end of the dwell. This trend is different from the thin specimen and indicates that the chemical cure shrinkage induced significant shear deformation that would result

Excerpt from ISBN 978-3-00-053387-7

in suppressed residual deformation. During cooling, the normal strain was significantly larger than shear strain as in the thin specimen. The spring-in angle was 0.36º for the thick specimen that is smaller than the thin one.

Next, the ratio of the shear to normal strain increments was calculated based on Eq. 7 and the result is shown in Figure 7. Assuming shear stiffness is quite low as in the liquid state, the through-thickness shrinkage in a corner part of an L-shaped part causes shear deformation to maintain the in-plane arc length. The shear strain for an L-shaped part with corner angle of ϕ can be geometrically calculated, and the shear/normal strain ratio in the flange is $\phi/2$. In Figure 7, the shear/normal ratio was about $\pi/4$ ($\sim$ 0.8) just after gelation at 200 min, which corresponds to a half angle of the curved area (i.e., $\pi/2$). The ratio significantly decreased down to almost 0 in the thin specimen, indicating that the shear stiffness greatly increased and shear deformation was suppressed. In contrast, the ratio was above 0.5 in the thick specimen throughout the 90 ºC holding. It means large shear deformation occurred in the thick specimen, resulting in smaller cure induced deformation. This result is consistent with the analysis conducted by Wisnom et al. [4] that showed larger shear strain and smaller residual deformation in thicker specimens. Although the analysis did not consider the effect of the flange, similar trend was captured in this study. The scatter after 300 min is caused by small increment in the normal and shear strains. During cooling, the shear/normal strain ratio was smaller than 0.2 in both

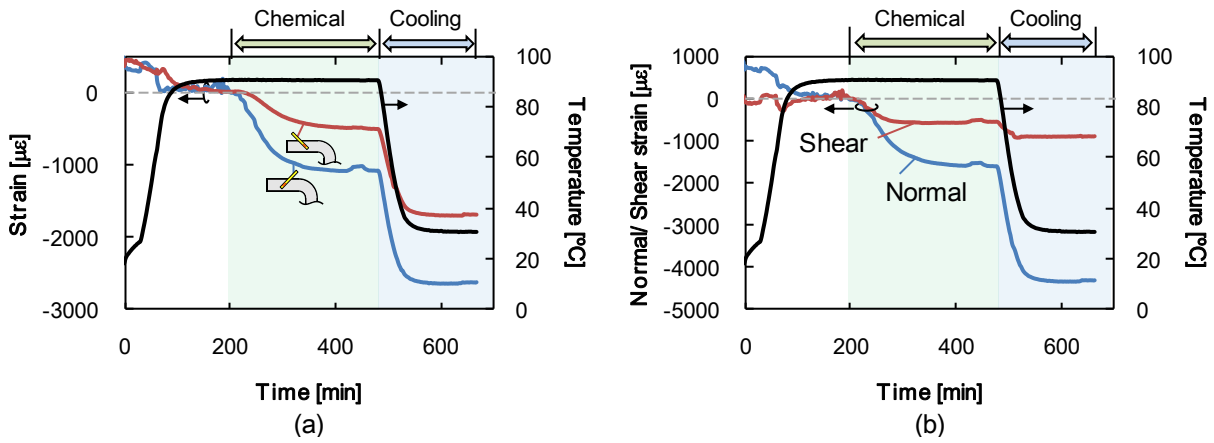

Figure 5. Cure process monitoring result of thin (20-ply) L-shaped specimen : (a) Measured strain and (b) Calculated normal and shear strains.

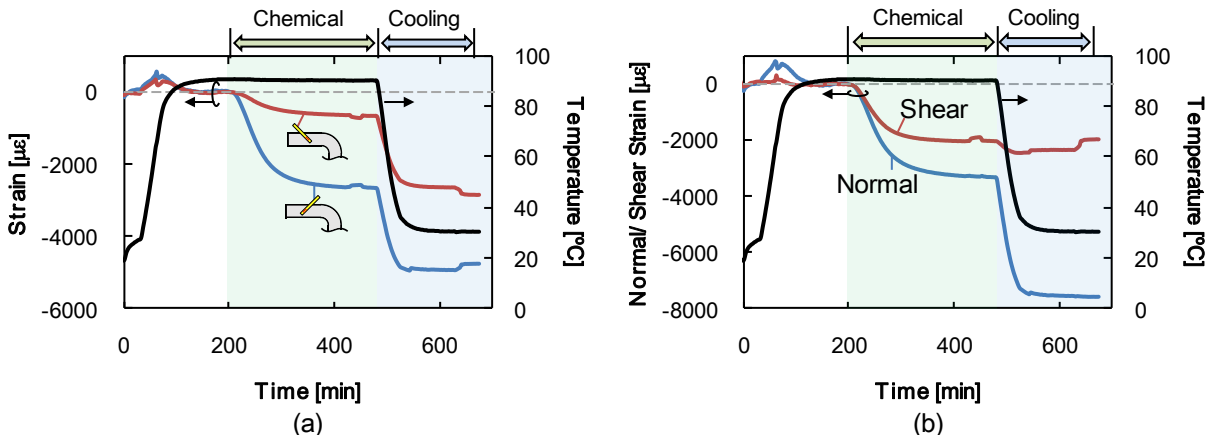

Figure 6. Cure process monitoring result of thick (64-ply) L-shaped specimen : (a) Measured strain and (b) Calculated normal and shear strains.

Excerpt from ISBN 978-3-00-053387-7

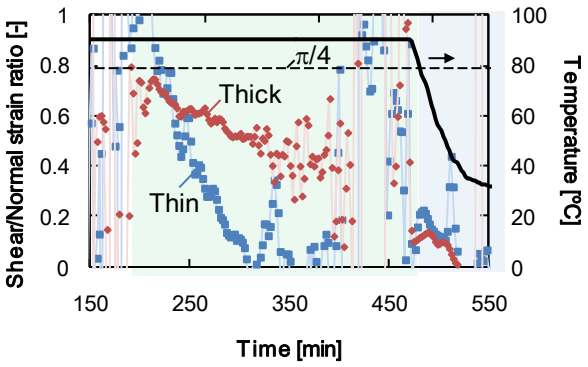

Figure 7. Shear/Normal strain ratio in thin and thick specimens.

thin and thick specimens. This was caused by high shear stiffness due to the glassy resin and the amount of the spring-in deformation during cooling would be the same in both of the specimens. The results shows that difference occurs only during curing in thin and thick specimens, implying that the chemical cure shrinkage significantly affected the difference in the spring-in angles.

Figure 8 (a) illustrates the numerically calculated shear/normal strain ratio as a function of the Young's modulus of the resin E_m. In our previous research, it was confirmed that the modulus increases up to a few hundred MPa during the 90 ºC holding. Thus, a gray vertical line is plotted at 200 MPa in the figure as the end of the 90 ºC dwell. In both thin and thick cases, the strain ratios decrease as cure proceeds from $\pi/4$ that is predicted with negligible shear stiffness. It reaches 0.2 in the thin case during cure process, whereas it decreases only down to 0.5 in the thick case. This numerical result is consistent well with the experiment data (Figure 7), confirming the validity of the experiment and showing larger shear deformation occurs in thick parts. In addition, Figure 8 (b) shows cure induced displacement at the flange end (Figure 4 (b)) when the out-of-plane normal strain of 1000 με is applied. The displacement increases as cure proceeds and the Young's modulus increases. Smaller displacement is generated in the thick part than the thin one because larger shear deformation occurs in the thick specimen as shown in the experiment and numerical results. This result explains the measured spring-in in the experiment, which was smaller in the thick specimen than the thin one.

4. Conclusion

Cure induced residual deformation is a serious problem for complex shaped composites. The fundamental mechanisms of the deformation are not clear due to the lack of internal state measurement methods. This research developed a fiber-optic-based multi-axial strain monitoring and investigated the effect of the part thickness on the strain development and residual deformation. First, thin and thick L-shaped specimens were fabricated and FBG sensors were diagonally embedded into the specimens. The sensor responses were monitored and the out-of-plane normal and shear strains were calculated. The result revealed that larger shear deformation was generated in the thick part than the thin one. 3D shape measurement after cure showed smaller spring-in in the thick part. It was because the larger shear deformation in the thick specimen suppressed the bending stress development that results in residual deformation. Then, FEA was carried out to further study the experiment results. The numerical result indicated that larger shear strain and smaller residual deformation in the thick part, showing the validity of the measurement. This research experimentally and numerically revealed that larger shear deformation is induced in thick specimens, reducing the residual deformations compared with thinner ones. Future work quantitatively investigates the relationship between the cure induced strain and residual deformation. Moreover, the effect of cure process will be studied using the proposed measurement method and optimal cure process will be proposed.

Excerpt from ISBN 978-3-00-053387-7

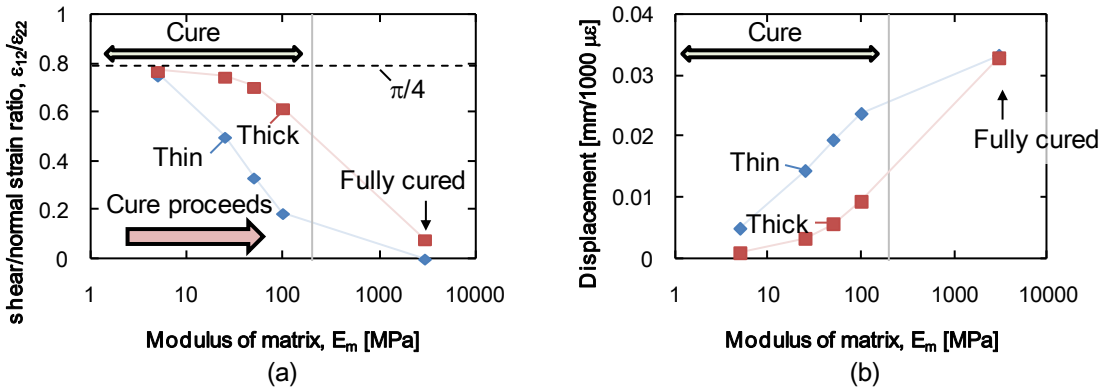

Figure 8. (a) shear/normal strain ratio, (b) displacement at edge when 1000 με out-of-plane normal strain is applied, as a function of Young's modulus of matrix.

Acknowledgments

This work was supported by Council for Science, Technology and Innovation (CSTI), Cross-ministerial Strategic Innovation Promotion Program (SIP), "Innovative Structural Material Project" (Funding agency: JST). K.T. also received funding from JSPS Grant-in-Aid for JSPS Fellows Number 26-5837. N.T. and S.M. were also partially supported by JSPS Grant-in-Aid for Scientific Research (S) Number 26220912.

References

[1] C. Albert, G. Fernlund. Spring-in and warpage of angled composite laminates. *Composites Science and Technology*, 62:1895–912,2002.

[2] E. Kappel. Forced-interaction and spring-in – Relevant initiators of process-induced distortions in composite manufacturing. *Composite Structures*, 140:217–29,2016.

[3] D.W. Radford, R.J. Diefendorf. Shape instabilities in composites resulting from laminate anisotropy. *Journal of Reinforced Plastics and Composites*, 12:58–75,1993.

[4] M.R. Wisnom, K.D. Potter, N. Ersoy. Shear-lag Analysis of the Effect of Thickness on Spring-in of Curved Composites. *Journal of Composite Materials*, 41:1311–24,2006.

[5] N. Ersoy, T. Garstka, K. Potter, M.R. Wisnom, D. Porter, G. Stringer. Modelling of the spring-in phenomenon in curved parts made of a thermosetting composite. *Composites Part A: Applied Science and Manufacturing*, 41:410–8,2010.

[6] K. Çınar, U.E. Ozturk, N. Ersoy, M.R. Wisnom. Modelling manufacturing deformations in corner sections made of composite materials. *Journal of Composite Materials*, 48:799–813,2014.

[7] K. Çınar, N. Ersoy. Effect of fibre wrinkling to the spring-in behaviour of L-shaped composite materials. *Composites Part A: Applied Science and Manufacturing*, 69:105–14,2015.

[8] C.K.Y. Leung, K.T. Wan, D. Inaudi, X. Bao, W. Habel, Z. Zhou, et al. Review: optical fiber sensors for civil engineering applications. *Materials and Structures*, 48:871–906,2015.

[9] S. Minakuchi. In situ characterization of direction-dependent cure-induced shrinkage in thermoset composite laminates with fiber-optic sensors embedded in through-thickness and in-plane directions. *Journal of Composite Materials*, 49:1021–34,2015.

[10] S. Minakuchi, S. Niwa, K. Takagaki, N. Takeda. Composite Cure Simulation Scheme Fully Integrating Internal Strain Measurement. *Composites Part A: Applied Science and Manufacturing*, 84:53–63,2016.

Excerpt from ISBN 978-3-00-053387-7